Journal of Pathology
J Pathol 2026
Published online 5 February 2026 in Wiley Online Library (wileyonlinelibrary.com) **DOI:** 10.1002/path.70034

ORIGINAL ARTICLE

Characterisation of bacteria-induced colitis and its modulation by probiotics in naked mole rats: a new mammalian model for acute inflammatory disease

Daniel W. Hart[1†], Aik Seng Ng[2,3†], Patrycja Gazińska[4], Robert Goldin[5], Purva Gopal[6], Nicolize O'Dell[7], Ahmad Zargar[8], Lior Pytowski[9], Shamir Montazid[3], Chiara Bardella[3], James E. East[10], Ian P. Tomlinson[3], Nadine Koch[11], Nigel C. Bennett[1] and Shazia Irshad[2,3*]

[1] *Mammal Research Institute, Department of Zoology and Entomology, University of Pretoria, Pretoria, Republic of South Africa*
[2] *Nuffield Department of Clinical Laboratory Sciences, Radcliffe Department of Medicine, University of Oxford, Oxford, UK*
[3] *Department of Oncology, University of Oxford, Oxford, UK*
[4] *Department of Oncology and Haematology, Faculty of Medicine, Wroclaw University of Science and Technology, Wroclaw, Poland*
[5] *Department of Metabolism, Digestion and Reproduction, Faculty of Medicine, Imperial College London, London, UK*
[6] *Department of Pathology, University of Texas Southwestern Medical Center, Dallas, Texas, USA*
[7] *Department of Paraclinical Sciences, Faculty of Veterinary Science, University of Pretoria, Pretoria, Republic of South Africa*
[8] *School of Medicine, Worsley Building, University of Leeds, Leeds, UK*
[9] *Pixel Biology Ltd., Oxford, UK*
[10] *Translational Gastroenterology and Liver Unit, Nuffield Department of Medicine, Experimental Medicine Division, University of Oxford, John Radcliffe Hospital, Oxford, UK*
[11] *Department of Medicine II, Munich, Germany*

**Correspondence to: S Irshad, Nuffield Department of Clinical Laboratory Sciences, Radcliffe Department of Medicine, University of Oxford, Level 4, Academic Block, John Radcliffe Hospital, Headington, Oxford OX3 9DU, UK. E-mail: shazia.irshad@ndcls.ox.ac.uk*

[†]These authors are equally contributions.

Abstract

Enteropathogenic bacteria are a major cause of morbidity and mortality globally. While mouse models have been indispensable in advancing our understanding of infectious enteric diseases, key differences in intestinal microbiota and immunobiology between mice and humans underscore the need for alternative mammalian models that better recapitulate human disease states. The naked mole rat (NMR), the longest-lived rodent and a model of healthy ageing, presents a unique opportunity. It possesses an exceptionally robust intestinal barrier, an abundance of goblet cells, a thicker mucin layer, and reduced gut permeability compared to mice. Additionally, the NMR gut microbiome exhibits compositional and functional features shared with human centenarians and traditional-lifestyle populations (e.g. Hadza hunter-gatherers), including an enrichment of health-associated taxa and metabolic pathways. Here, we leverage this model to show that systemic *Citrobacter braakii* infection is associated with colonic inflammation and epithelial injury that closely mimics human haemorrhagic colitis. Infected NMRs develop mucosal erosions, ulcerations, depletion of goblet cells, expansion of proliferative compartments, and active inflammation in the lamina propria. Without intervention, systemic inflammation associated with sepsis ensues and results in high mortality. Furthermore, we demonstrate the utility of this model for therapeutic testing by showing a strong effect of a probiotic cocktail comprising lactobacilli, bifidobacteria, streptococci, and enterococci. Treatment with this cocktail promoted mucosal healing, restored intestinal homeostasis, and exerted an anti-inflammatory effect. Taken together, we establish the NMR as a translatable model for investigating disease mechanisms in infectious colitis, including disruptions in mucosal barrier permeability, gut microbial ecology, and local and systemic immune regulation, as well as for testing functional probiotic strains as potential therapeutics.

Keywords: naked mole rats; infectious colitis; *Citrobacter braakii*; inflammation; epithelial atypia; goblet cell depletion; sepsis; probiotics; mucosal healing

Received 4 July 2025; Revised 27 November 2025; Accepted 31 December 2025

No conflicts of interest were declared.

Introduction

Laboratory mice have served as powerful tools for studying host–enteropathogen infections and underlying mechanisms of acute and chronic inflammatory diseases of the gut. These include genetically engineered mice, congenic models, chemically induced and immune cell transfer models, and gnotobiotic and gut infection

models, among others [1–12]. These models have been instrumental in deciphering the role of uncontrolled bacterial colonisation, epithelial barrier disruption, and unregulated immune stimulation in inflammatory diseases. Furthermore, mouse models have also been used in evaluating novel therapeutics [13–16]. There are, however, considerable differences in the innate and adaptive immunity of mice and humans, reflecting the development of divergent strategies to combat pathogenic challenges within species-specific ecological niches [17–19]. Moreover, housing laboratory mice in specific pathogen-free (SPF) conditions profoundly affects the murine basal immune state [20–24]. Similarly, there are significant differences in the presence of specific bacterial species between laboratory mice and the human gut microbiota [25]. Given the taxonomic complexity, trans-kingdom interactions within the metagenome, and their role in driving local and systemic pro-inflammatory diseases, new experimental models are needed to capture the full composition and diversity of the luminal bacterial community. One approach is to include other rodent species with diverse gut microbiota, immune cell repertoire, and intestinal physiology that are closer to those of humans.

The naked mole rat (NMR), *Heterocephalus glaber*, is the longest-lived rodent, with a maximum lifespan of > 30 years [26], that has gained much attention as an anti-cancer and anti-ageing model organism. These animals exhibit an extremely low cancer incidence [27–32] and an attenuated decline in physiological functions with age, including in the reproductive [28], cardiovascular [33], and gastrointestinal systems [34]. Several aspects of NMR biology make it a highly suitable mammalian model for exploring gut homeostasis that is relevant to understanding human intestinal physiology and associated diseases. Firstly, similar to human colons [35], NMRs' colons have a thicker protective mucin layer compared to mice [36,37], suggesting that NMRs have the potential to provide novel insight into the regulation of the penetrability properties of the inner mucus and in testing novel therapeutics for enteric infections and gut inflammation in humans. We have also recently shown that the cellular kinetics of *Lgr5*-expressing crypt-based columnar cells in the NMR colon are almost identical to human *LGR5*$^{+}$ cells while being significantly slower than those observed in mice [36]. This makes NMRs ideal for studying inflammation-induced effects on intestinal stem cells and regeneration efficiency during remission in humans. NMRs also make an interesting model for studying the host–microbiota interaction, with faecal and caecal samples of these animals showing Firmicutes and Bacteroidetes as the dominant bacterial phyla, which are similar to those in humans [38–41]. Even more interestingly, NMRs also possess a high load and diversity of Spirochetaceae and Mogibacteriaceae, taxa found in human populations with unique diets, such as Hadza hunter-gatherers [42,43], or in individuals with exceptional longevity, such as supercentenarians [44].

The NMR haematopoietic system has also evolved unique features, with key differences compared to mice [45–48]. For example, the NMR splenic and circulating immune cell repertoire shows a higher myeloid-to-lymphoid ratio compared to mice [45]. A similar myeloid prevalence is seen in humans [17]. A higher number of granulocytes found in NMRs are mostly neutrophils, including a novel lactoferrin-high neutrophil subset that expresses several antimicrobials and is highly responsive to a bacteria-mimicking challenge [45]. Compared to their mouse counterparts, NMR macrophages have a greater phagocytic capability and produce higher pro-inflammatory cytokines [49,50]. One of the most striking aspects of the NMR immune system is the absence of natural killer (NK) cells, which has been associated with the high susceptibility of this species to viral infections [45]. This likely reflects weaker viral selection pressures due to limited exposure to airborne viruses in their subterranean habitat [51,52]. Furthermore, NMRs also do not show an age-associated increase in blood leucocytes and platelets, which could reduce chronic inflammation and delays age-associated thrombosis [46]. Additionally, several inflammaging-related pathways appear to be down-regulated in older NMRs [46].

Here we report the spontaneous development of bacterially induced acute colitis in NMRs after a sporadic outbreak of *Citrobacter braakii* infection in our captive NMR colonies. Infected NMRs displayed several clinical and histopathological features characteristic of murine [53] and human colitis [54]. These included inflammation in the mucosal and submucosal layers of the colon, accompanied by oedema, loss of goblet cells, hyperplasia, and ulcerations. Treatment of NMRs with probiotics alleviated symptoms of colitis and reversed all the histopathological features in the colon, including an increase in goblet cells and reduction in the hyperproliferation of crypt cells to levels seen at homeostasis in healthy NMRs. Distinct from their use in anti-ageing and anti-cancer research, our new findings highlight the potential of NMRs as an experimental mammalian model for understanding epithelial barrier function defects, gut dysbiosis, and inflammation triggered by enteric infections and for testing therapeutic modalities.

Materials and methods

Animal ethics

All scientific procedures involving NMRs were carried out with approval from the Animal Ethics Committee at the University of Pretoria under licenses EC034-18, NAS046-19, NAS199-2020, NAS289-2020, NAS017-2021, and NAS022-2021. Additionally, approval was obtained from the Department of Agriculture, Forestry, and Fisheries (DAFF) under Section 20 (SDAH-Epi-20111909592, SDAH-Epi-21021810221 and SDAH-Epi-21021810222, SDAH-Epi-20072707041).

Naked mole rat husbandry

NMRs were housed in two separate, non-sterile animal facilities within the Department of Zoology and Entomology

at the University of Pretoria. They inhabited non-sterile tunnel systems composed of interconnected Perspex chambers, with wood shavings provided as nesting material. All NMRs remained within their respective colonies, except when removed for breeding or experimental procedures, in accordance with standard laboratory operating protocols. Animals were weighed regularly, and various biological samples, including faecal matter and blood, were collected as part of specific experimental protocols and general standard operating procedures. The ambient conditions in the NMR housing rooms were maintained at a temperature range of 29–32 °C, with a relative humidity of 40–60%, replicating the underground burrow environments of their natural habitat. NMRs were provided with a daily *ad libitum* diet consisting of chopped fresh fruits and vegetables (e.g. apple, sweet potato, cucumber, and capsicum), supplemented once daily with ProNutro (Bokomo, Cape Town, South Africa) [55]. As NMRs obtain sufficient hydration from their food, no additional drinking water was provided. The health status of all NMRs was monitored daily.

Isolation of symptomatic NMRs

Animals that presented with skin discolouration, weight loss, diarrhoea, bloody stool, or recumbency were removed from their colonies and housed individually in plastic chambers with sterilised wood shavings as nesting material. These animals were fed a daily *ad libitum* diet of chopped fresh fruits and vegetables (e.g. apple, sweet potato, cucumber, and capsicum), along with a bi-daily supplement of ProNutro (Bokomo, Cape Town, South Africa).

Probiotic treatment of NMRs

Symptomatic NMRs presenting with skin discolouration, weight loss, diarrhoea, bloody stool, or recumbency were removed from their colonies and housed individually. In addition to a base diet of fresh fruits and vegetables provided *ad libitum*, each animal received a bi-daily supplement of 0.75–1.0 g of ProNutro (Bokomo, Cape Town, South Africa) blended with 0.1 g of a seven-strain probiotic cocktail (Protexin, Kyron, South Africa), achieving a 1:10 ratio. The entire supplement was consistently consumed, confirming a daily probiotic intake of 0.1 g per animal. This dietary method was selected to minimise handling stress in clinically affected animals. A separate colony of healthy NMRs ($n = 10$) was group-housed and provided with the same probiotic-ProNutro mixture (maintaining the 1:10 ratio) *ad libitum*. In this setting, individual intake was not measured, and consumption was self-regulated by the colony. The Protexin probiotic cocktail contained the following strains: *Lactobacillus plantarum*, *Lactobacillus delbrueckii* subsp. *bulgaricus*, *Lactobacillus acidophilus*, *Lactobacillus rhamnosus*, *Bifidobacterium bifidum*, *Streptococcus salivarius* subsp. *thermophilus*, and *Enterococcus faecium*.

Tissue collection and processing

NMRs were euthanised according to approved protocols as previously described [36]. Before euthanasia, whole blood was collected. The bleed site was first cleaned by thoroughly swabbing the tail with Biotaine (0.5% chlorhexidine gluconate, 70% ethanol; Braun Medical, reg. no. 33/13.1/0526) and allowing it to dry. A sterile blade was then used to pierce the tail, and blood was collected using an EDTA-coated microhaematocrit capillary tube. The collected blood was immediately transferred to a sterile EDTA tube for further analysis.

Next, intestines were excised from the abdominal cavity and subdivided into four segments: the duodenum, jejunum, ileum, and colon as reported previously [36]. All portions of the intestine were then flushed with a 1× PBS (Phosphate-Buffered Saline) solution, using a P1000 pipette to remove any faecal material. Measurements were taken to determine the length of the intestinal tract. Each segment of tissue was longitudinally incised with a gut-cutting device, and the edges were affixed to a 3-mm filter paper with the luminal side facing upwards. Tissues were fixed overnight in 10% neutral buffered formalin at room temperature. Fixed tissues were then rolled up using the Swiss-rolling technique and transferred to 70% ethanol for storage at 4 °C. Subsequently, formalin-fixed Swiss rolls were dehydrated through progressively increasing ethanol concentrations, cleared with xylene, and embedded in paraffin wax.

Liver and lung samples were excised, collected in 1× PBS, and sent immediately for biochemical and pathological assessment to the Laboratory Diagnostic Services at the Department of Veterinary Tropical Diseases, University of Pretoria. Tissues were subsequently fixed in formalin and paraffin-embedded for further histological evaluation.

Finally, prior to any staining, paraffin blocks were sectioned at a thickness of 4 µm using a microtome (Leica, Illinois, USA) and mounted on SuperFrost Plus slides (VWR, 6310108, New Hampshire, USA) and dried overnight. Tissue sections were baked at 60 °C (1 h), deparaffinised by immersing slides in xylene (two times, 10 min each), and subsequently rehydrated in 100% ethanol (two times, 5 min each), 95% ethanol (2 min), 70% ethanol (2 min), 50% ethanol (2 min), and distilled water (5 min).

Diagnostic testing and identification of *C. braakii*

Tissue samples (liver and lung) were processed for bacteriological analysis by the Laboratory Diagnostic Services at the Department of Veterinary Tropical Diseases, University of Pretoria, using standard qualitative culture methods. In brief, sterile swabs were used to sample the inner surface of dissected tissues, which were then inoculated onto blood agar and MacConkey agar plates in parallel lines to assess the distribution and density of bacterial colonies. Plates were incubated aerobically at 37 °C for 18–24 h. This protocol allowed for

the growth of both aerobic and facultative anaerobic bacteria. The severity of growth for each isolate was determined semi-quantitatively by visual inspection, estimating the number and density of colonies distributed along the streak lines, and categorised as light, moderate, or heavy growth according to standard laboratory diagnostic protocols.

The predominant bacterial isolate from liver cultures, which exhibited heavy growth, was selected for further identification through Gram staining and a series of biochemical tests, including oxidase, catalase, and indole tests. Based on its biochemical profile, final confirmation of the species was achieved using the API 10 S system following the manufacturer's instructions.

H&E staining

H&E staining was performed as described previously [36]. After deparaffinisation and rehydration, sections were stained with Harris' Haematoxylin (Merck, HHS32, Darmstadt, Germany) (2 min 45 s) followed by a 5-min wash under running tap water. Subsequently, slides were immersed in 95% ethanol (10 times) before counterstaining with eosin solution (Merck, 117,081, Darmstadt, Germany) for 3 min. The tissue sections were then dehydrated in 95% ethanol (15 s) and 100% ethanol (two times, 15 s each), immersed in xylene (two times, 5 min each), and finally coverslipped with DPX Mountant (Merck, 06522, Darmstadt, Germany).

Alcian blue staining

Alcian blue staining was performed as described previously [36]. Following deparaffinisation and rehydration, sections were immersed in 3% acetic acid solution for 3 min before being stained with Alcian blue 8GX solution (pH 2.5) (Merck, A5268, Darmstadt, Germany) for 30 min. The tissue sections were then washed under running tap water for 5 min and counterstained with Nuclear Fast Red (Merck, N3020, Darmstadt, Germany) for 5 min. Following a 1-min wash in running tap water, the tissue sections underwent dehydration in ethanols, immersion in xylene, and finally coverslipping with DPX Mountant (Merck, 06522, Darmstadt, Germany).

Immunohistochemistry

Following deparaffinisation and rehydration, endogenous peroxidase activity was quenched by incubating sections in 3% H_2O_2 (Merck, 8222871000, Darmstadt, Germany) for 20 min. A heat-mediated antigen retrieval was then performed by boiling sections in 1× target retrieval solution, Citrate pH 6.0 (Agilent Dako, S236984-2, Santa Clara, CA, USA) for 10 min. Slides were then allowed to cool to room temperature in the same solution. Next, tissue sections underwent permeabilisation through incubation with 1× PBSTX (0.1% Triton X-100) for 10 min. All sections were then blocked for 1 h at room temperature using 5% serum, which matched the species of the secondary antibody. Primary antibodies were prepared and diluted in antibody diluent (1% BSA prepared in 1× PBS) and applied to tissue sections for incubation at 4 °C, overnight in a humidified chamber. After three washes with 1× PBST (0.1% Tween20 in 1× PBS), biotinylated secondary antibodies prepared in antibody diluent were applied to slides and incubated for 1 h at room temperature in a humidified chamber. Target detection was performed using Avidin/Biotinylated enzyme Complex (ABC) kit (Vector Laboratories, PK-6101, CA, USA) and developed the signal using a 3,3'-diaminobenzidine (DAB) solution (R&D Systems, 4800-30-07, Minneapolis, MN, USA). Lastly, tissue sections were counterstained with Harris' Haematoxylin (Merck, HHS32, Darmstadt, Germany) for 5 s and underwent dehydration in 70, 90, and 100% ethanol for 15 s each, immersed in xylene, and coverslipped with DPX Mountant (Merck, 06522, Darmstadt, Germany). A list of primary antibodies used is provided in supplementary material, Table S1.

Brightfield microscopy

Brightfield images of tissue sections were captured on an Olympus BX51 microscope coupled with an Olympus DP70 camera system using DP controller software. Images were captured using 4×, 10×, 20×, and 40× objective lenses.

Quantification of blood immune cells

Complete blood counts were performed on NMRs whole blood samples in an automated haematological analyser (ADVIA 2120i Siemens, Dublin, Ireland) at the Clinical Pathology unit of the Department of Companion Animal Clinical Studies, Faculty of Veterinary Science, University of Pretoria. In brief, blood samples were mixed with ADVIA 2120i BASO reagent, which contains acid and surfactant to haemolyse the red blood cells. The white blood cells were then analysed using two-angle laser light scatter signals to obtain the total leucocyte counts. Next, the analyser used a peroxidase method to classify and quantitatively measure the total leucocyte count and differential counts (neutrophils, lymphocytes, monocytes, eosinophils, large unstained cells, and basophils) based on cell-specific constituents when the cells are treated with peroxidase stain.

Measurement of muscle layer thickness

Colonic tissue sections from healthy, infected, and treated NMRs were fixed in formalin, embedded in paraffin, and stained with H&E using standard protocols described earlier. Entire sections were digitally scanned at 40× resolution (0.23 μm/pixel) using a Hamamatsu NanoZoomer S60v2 slide scanner (Hamamatsu Photonics, Hamamatsu City, Japan). The thickness of the muscularis mucosa and muscularis propria was quantified using the annotation and measurement tools in Fiji (Image J). For each animal, the region of maximum thickness (μm) for each muscle layer

was identified throughout the gut roll. Next, three separate measurements were taken per animal, and the mean was taken to give a representative value per layer per group. This 'maximum thickness' approach was used to assess the potential for focal hypertrophy or atrophy in infected and treated animals compared to healthy ones.

Quantification of goblet cell surface area

Intestinal tissue sections from infected, treated, and healthy control NMRs were fixed in formalin and embedded in paraffin. Sections were stained with Alcian blue to visualise acidic mucins within goblet cells. To quantify goblet cells, entire tissue sections were digitally scanned at 40× resolution (digital magnification: 0.23 µm/pixel) using a Hamamatsu NanoZoomer S60 slide scanner (Hamamatsu Photonics). The surface area of individual goblet cells was measured using NDP.view2 Plus (U12388-02) annotation tool. For each animal, at least 30 goblet cells were measured across three randomly selected crypts from the colon. The mean goblet cell area was then calculated for each experimental group (healthy, infected, and treated NMRs) and compared.

Wright–Giemsa staining

Blood smears from EDTA blood were prepared on glass slides and subsequently stained with a Wright–Giemsa stain using an automated stainer (Aerospray Hematology Pro, EliTech Group, Utah, USA). Photomicrographs were captured using a Zeiss Axio Lab A1 microscope (Jena, Germany) with a Zeiss Axiocam ERc5s using Zeiss Zen software.

Phylogenetic analysis

The sequences for each of seven housekeeping genes (*adk*, *fumC*, *gyrB*, *icd*, *mdh*, *purA*, and *recA*) were extracted for the following enteric bacteria: *C. braakii* strain MiY-A (accession number: NZ_CP045771), *Citrobacter rodentium* ICC168 (accession number: NC_013716.1), *Citrobacter koseri* ATCC BAA-895 (accession number: NC_009792.1), *Cronobacter sakazakii* ATCC BAA-894 (accession number: NC_009778.1), *Escherichia coli* O127:H6 str. E2348/69 (accession number: NC_011601.1), *E. coli* O157:H7 str. Sakai (accession number: NC_002695.2), *E. coli* str. K-12 substr. MG1655 (accession number NC_000913.3), *Klebsiella variicola* (strain: LEMB11) (accession number: NZ_CP045783.1), *Pectobacterium atrosepticum* SCRI1043 (accession number: NC_004547.2), *Salmonella enterica* subsp. *enterica serovar* Enteritidis str. P125109 (accession number: NC_011294.1), *Salmonella enterica* subsp. *enterica* serovar Typhi str. CT18 (NC_003198.1), *Salmonella enterica* subsp. *enterica* serovar Typhimurium str. LT2 (accession number: NC_003197.2), *Yersinia enterocolitica* subsp. *enterocolitica* 8081 (accession number: NC_008800.1), and individually aligned using MUSCLE [56]; they were subsequently concatenated. MEGA11 was used to identify the best phylogenetic model to fit the data using a maximum-likelihood algorithm. A phylogenetic tree was constructed using the maximum-likelihood method using the recommended General Time Reversible (GTR) plus Gamma model distributed with invariant sites. The reliability of the tree was estimated with the bootstrap method with replicates set at 500 and was rooted using an outgroup comprising *Yersinia* and *Pectobacterium*. Genome sequence homology was performed using the Basic Local Alignment Search Tool (BLAST).

Statistical analysis

All quantitative data are presented as mean ± SEM. Statistical differences between two experimental groups were analyzed by a two-tailed unpaired Student's *t*-test or a Mann–Whitney test using GraphPad Prism 10.2.0. The levels of significance for individual data sets are indicated in the corresponding figure legends.

Results

Spontaneous disease outbreak in NMR colonies

NMRs were housed in two non-sterile housing facilities and monitored according to standard husbandry protocols (see Materials and methods). At one facility housing 145 NMRs, individuals from three separate breeding colonies ($n = 9$; non-breeders) began exhibiting clinical signs of morbidity, including a hunched posture, reluctance to move, recumbency, and skin discolouration. Their condition progressively worsened, culminating in death within 9 weeks of symptom onset. One week later, we identified a second cohort of adult NMRs ($n = 7$; five female, two male) that presented with similar symptoms, including skin discolouration and lethargy (Figure 1A). These individuals were immediately separated from their colonies and enrolled in this study for comprehensive disease phenotyping, as outlined in supplementary material, Figure S1.

The affected NMRs ($n = 7$) continued to deteriorate, developing additional symptoms such as rectal bleeding and severe dehydration (Figure 1A). Supportive rehydration with saline did not improve the condition. Over the course of the disease, these NMRs experienced severe weight loss, with a cumulative reduction of approximately 30% from their initial body mass by week 10, progressing to a 55% loss by week 15 (Figure 1B). In contrast, both healthy control groups, adult colony-dwelling ($n = 20$; 12 female, eight male), and adult solitary-housed NMRs ($n = 10$; three female, seven male), maintained or gained body mass over the 32-week observational period (Figure 1B). The stool consistency of symptomatic NMRs also deteriorated progressively, transitioning from normal, hard pellets (Score 0) to a soft, watery consistency (Score 1) by week 6 (Figure 1C). This worsened further, with stools appearing red/brown (score 2) by week 10 and becoming bloody and watery (Score 3) by week 14 (Figure 1C). At the 14-week mark, two NMRs became immobile with

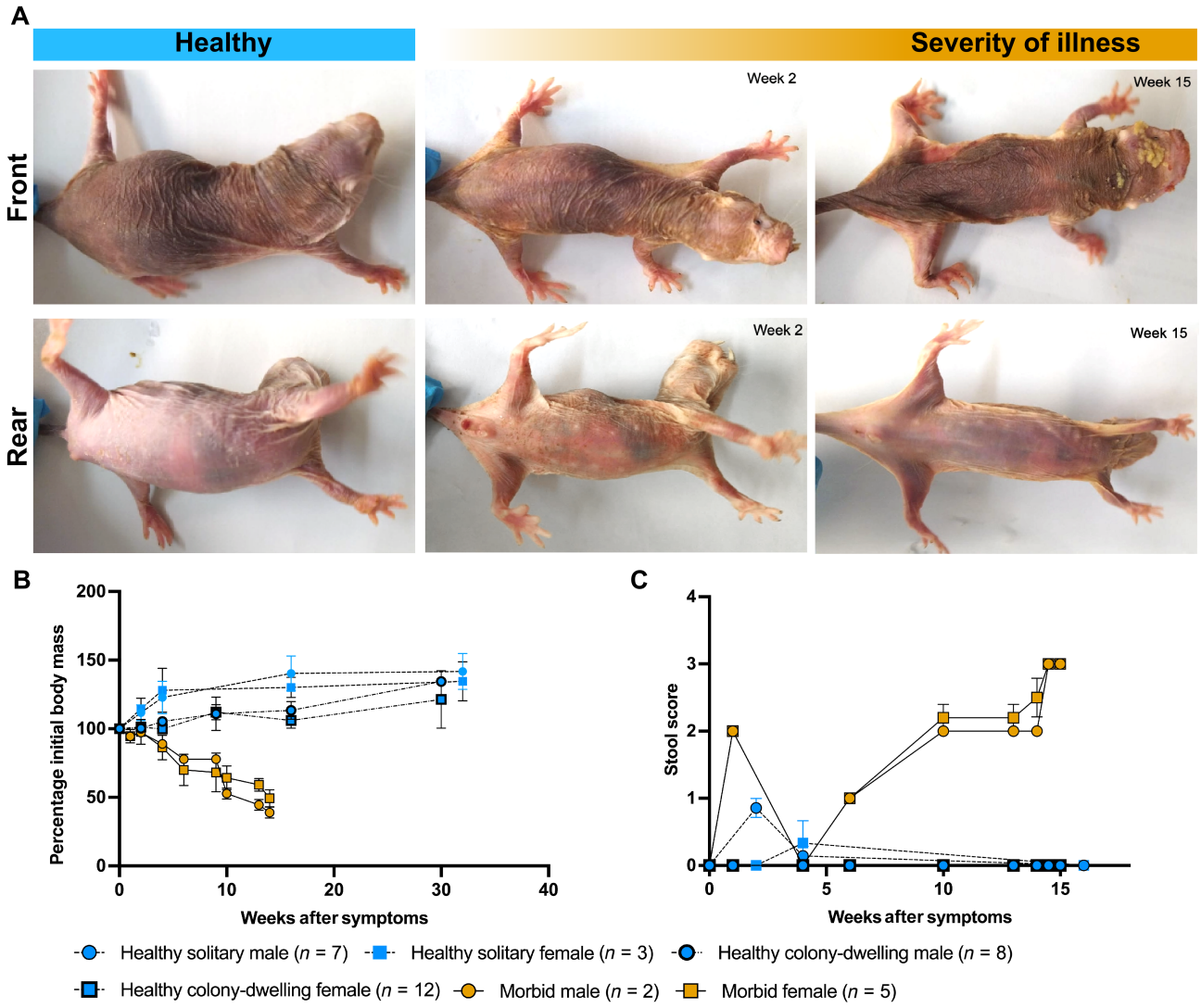

Scoring Criteria			
Stool Score	Stool Description		
	Hardness	Water Content	Colour
0	Hard	Dry	Black
1	Soft	Slightly watery	Yellow
2	Soft	Watery	Red/brown
3	N/A	Bloody diarrhoea	Red/yellow

Figure 1. Spontaneous disease outbreak in NMR colonies. (A) Gross morphological changes in symptomatic NMRs over 15 weeks. (B) Changes in body mass of sick NMRs compared to healthy NMRs. Each data point represents mean body mass (± SEM) for sick NMRs [$n = 7$; five females (F) and two males (M); non-breeders; median age: 33 months, interquartile range (IQR): 23–42], healthy colony-dwelling NMRs ($n = 20$; 12 F, eight M; non-breeders; median age: 36 months, IQR: 21–59), and healthy NMRs in solitary confinement ($n = 10$; three F and seven M; non-breeders; median age: 28 months, IQR: 23–36). (C) (Top) Graph showing changes in stool score over a 16-week period for sick ($n = 7$), healthy colony-dwelling ($n = 20$), and healthy solitary ($n = 10$) NMRs. Each data point represents the mean stool score (± SEM). (Bottom left) Representative stool samples from healthy (score 0) to symptomatic NMRs with increasing disease severity (scores 1–3). (Bottom right) Metrics used for scoring stool samples.

laboured breathing and were euthanised for detailed histopathological and biochemical analysis of blood, liver, lung, and colonic tissues. The remaining affected NMRs ($n = 5$) reached this end stage by week 17 and were processed similarly for tissue collection and analysis.

NMRs are susceptible to *C. braakii* infections, a mole rat enteropathogen analogous to *Citrobacter rodentium* in mice and *Escherichia coli* in humans

To characterise the cause of morbidity in NMRs, we examined the blood and various tissues from these

animals. First, Giemsa-stained blood smears from diseased NMRs revealed rod-shaped bacteria, both extracellularly (Figure 2A, left, black arrows) and within monocytes (Figure 2A, left, blue arrow). We also observed occasional bacteria with coccoid morphology (Figure 2A, right, black arrow). The observation of bacteraemia, a well-known trigger for emergency myelopoiesis [57–59], prompted us to quantify the resulting systemic inflammatory response in the blood of infected NMRs. Analysis of the peripheral blood from healthy solitary NMRs ($n = 4$) established a baseline profile, with lymphocytes (43%) and mature neutrophils (52%) as the predominant leucocytes, consistent with previous reports [47] (Figure 2B). Other cell types, including immature neutrophils, basophils, and eosinophils were absent or minimal, while monocytes were present at low levels (3%). In stark contrast, blood from infected NMRs ($n = 5$) revealed a signature of systemic infection, characterised by a marked 37% decrease in mature neutrophils and concurrent increases in immature neutrophils (5%) and monocytes (28%) (Figure 2B). The proportions of lymphocytes, basophils, and eosinophils remained largely unaltered. Taken together, these observations demonstrate that systemic bacterial infection in NMRs triggers emergency myelopoiesis, evidenced by the release of immature neutrophil precursors into the periphery and a pronounced shift in myeloid differentiation towards the monocyte lineage. This systemic host immune response aligns with those reported in mice and human sepsis [60,61].

Further histological examinations of solid tissues in infected NMRs revealed multiple small foci of necrosis and inflammation in the liver (supplementary material, Figure S2A). The lungs also displayed moderate interstitial pneumonia, characterised by mononuclear cell infiltration of the alveolar walls (supplementary material, Figure S2B). To identify the causative pathogen, bacterial cultures grown from affected liver samples were plated on blood agar and MacConkey agar and yielded a pure, heavy growth of a single bacterial type, characterised by a uniform colony morphology on both blood and MacConkey agar, with no other distinct colony types observed. The predominant isolate was identified as Gram-negative rods that were oxidase-negative, catalase-positive, and indole-negative, classifying it within the Enterobacteriaceae family. Final confirmation using the API 10 S system identified the bacterial species as *C. braakii*. The absence of cultured coccoid bacteria from the liver, despite their visualisation in blood smears, suggests they were present in the bloodstream but did not establish a significant infection in the liver, which was predominantly colonised by *C. braakii*.

Given the early clinical signs of enteric disease (rectal bleeding, bloody stool, diarrhoea), we hypothesised that the systemic *C. braakii* infection originated from the gastrointestinal tract. To assess the potential of this liver isolate to act as an enteric pathogen, we determined its relationship to other known enteric bacteria. We constructed a phylogenetic tree using DNA sequences of seven housekeeping genes (*adk*, *fumC*, *gyrB*, *icd*, *mdh*, *purA*, and *recA*), as reported previously [62]. Pairwise whole-genome comparison revealed high sequence homology between *C. braakii* and *E. coli* K-12 (89.54%), *C. braakii* and *Citrobacter rodentium* (89.80%), and *C. rodentium* and *E. coli* K-12 (90.13%) (supplementary material, Figure S3). This close genetic relationship demonstrates that *C. braakii* is closely related to these members of the Enterobacteriaceae. This shared genetic background provides a plausible basis for it to employ similar pathogenic strategies. This is significant given that *C. rodentium*, a natural murine pathogen, is the dominant model for studying human intestinal disease caused by enteropathogenic and enterohaemorrhagic *E. coli* (EPEC/EHEC) [63–65]. Therefore, we propose that *C. braakii* infection in NMRs could serve as a surrogate model for EPEC/EHEC-like disease.

Having established the genetic relatedness of *C. braakii* to known enteric pathogens, we next sought histological evidence of gut colonisation to assess whether the cause of septicaemia resulted from the translocation of enteropathogenic bacteria from the gut into the bloodstream. To this end, we analysed the intestines of infected NMRs ($n = 7$) for the presence of Gram-negative and Gram-positive bacteria, using anti-lipopolysaccharide (LPS) and anti-lipoteichoic acid (LTA) antibodies. Given that we used formalin fixation and not Carnoy's solution for tissue processing, which would have preserved the mucus layer, our analysis was limited to detecting bacteria that had breached this layer and were in direct contact with or had invaded the epithelial tissue. Positive LPS staining was detected in close proximity to the intestinal epithelial surface of the caecum and the colon of infected NMRs (Figure 2C). Conversely, no LTA staining was seen in these tissues from infected NMRs (Figure 2D). The absence of detectable Gram-positive bacteria at the epithelium, concurrent with a heavy burden of Gram-negative bacteria, is consistent with a state of microbial dysbiosis where the invading Gram-negative pathogen dominated the colonic niche. Taken together, our findings support a model of pathogenesis where damage to the lower gastrointestinal tract, evidenced by early clinical signs and the presence of Gram-negative bacteria at the colonic epithelium, facilitated the translocation of enteric bacteria into the bloodstream. The subsequent isolation of *C. braakii* as a pure, heavy growth from the liver indicates that it was the primary pathogen responsible for the resulting septicaemia and end-organ damage. While our methodology does not definitively rule out an initial role for another undetected pathogen, the most parsimonious explanation is that the observed Gram-negative colonic invasion represents *C. braakii*, which then seeded the systemic infection.

C. braakii-infected NMRs exhibit extensive intestinal epithelial damage

We next focused our efforts on characterising the intestinal histopathology in *C. braakii*-infected NMRs. The

small bowel in infected animals was largely unaffected, with only mild changes detected in the most distal regions of the small intestine (data not shown). In contrast, the entire colonic mucosa exhibited extensive architectural distortions in infected NMRs (Figure 3A). Epithelial atypia in all infected NMR colonic tissues

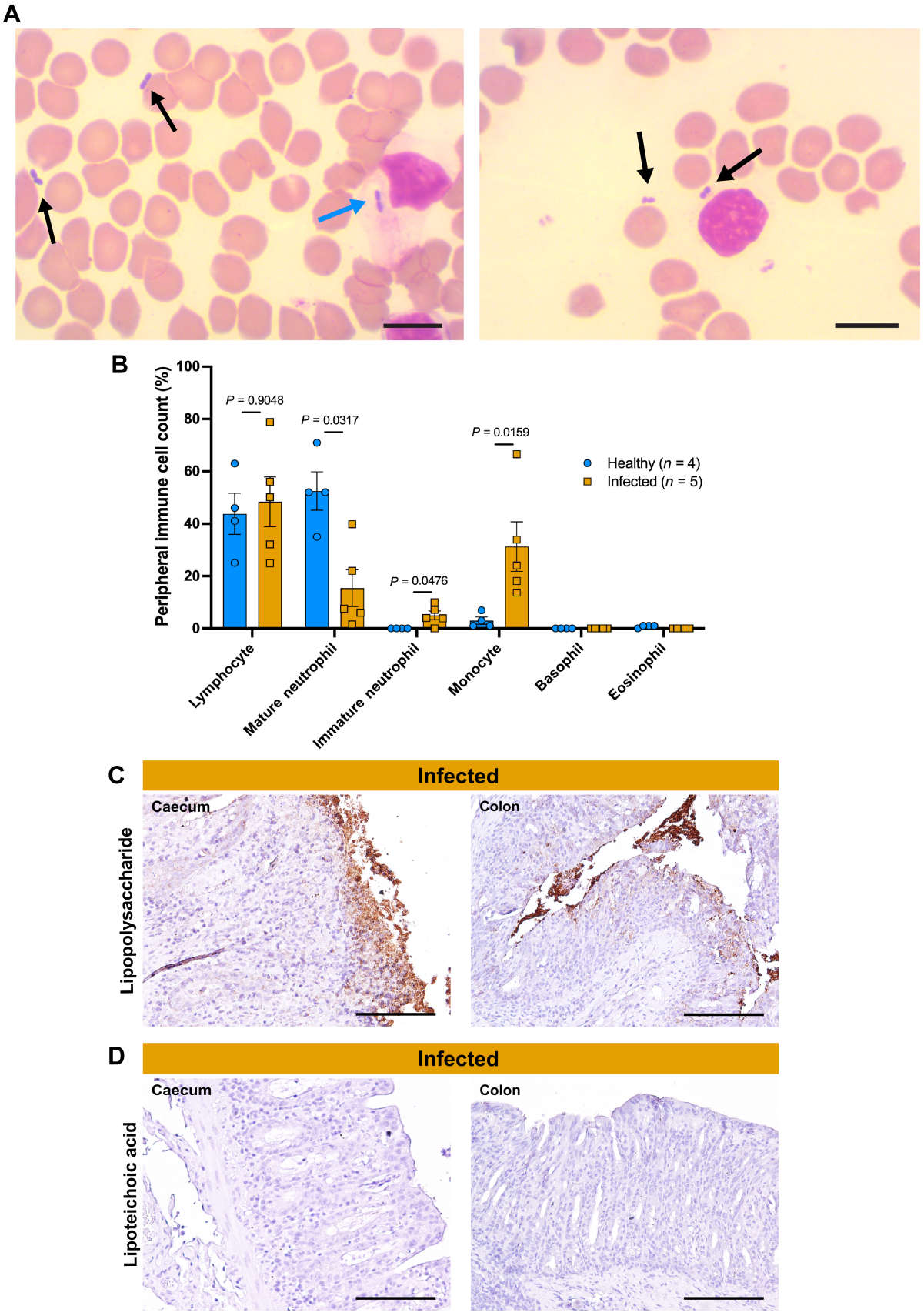

Figure 2 Legend on next page.

included crypt loss in some regions (Figure 3B), while crypt elongation was observed in others (Figure 3C). More specifically, crypt loss was observed in 16–60% of the entire colon in infected NMRs (Figure 3D), while crypt elongation was detected in 11–60% of the colon (Figure 3E). Other common epithelial abnormalities included crypt abscesses (supplementary material, Figure S4A), surface erosion and ulceration (supplementary material, Figure S4B, arrowheads), and crypt herniation (supplementary material, Figure S4C, arrowhead).

The extent of epithelial damage and mucosal architectural changes was scored by three independent pathologists using Swiss rolls of colonic tissue (supplementary material, Figure S4D) from all infected animals, based on established criteria for intestinal inflammation models [6,66–68], which is summarised in supplementary material, Figure S4E. Based on this scoring, 29% of infected animals exhibited isolated focal epithelial damage, 57% displayed extensive tissue damage including mucosal erosions and ulcerations, while 14% showed extensive damage deep into the bowel wall (Figure 3F, left). The percentage of epithelial surface involvement varied from 1–25% in 14% of animals to 26–50% in 57%, and 51–75% in the remaining 29% of infected NMRs (Figure 3F, right). Furthermore, we also observed a significant increase in the maximum thickness of both the muscularis mucosa and the muscularis propria in infected NMR colons, which were 225% and 48.5% thicker, respectively, than those of healthy controls (Figure 3G).

Colonic inflammation in *C. braakii*-infected NMRs

Comprehensive characterisation of inflammatory responses in NMRs is currently constrained by limited cross-reactivity of commercially available antibodies against immune cell markers. In the absence of reliable immunohistochemical staining for specific immune subtypes (including CD4, CD8, CD68, CD56, CD20, or FOXP3), we relied on a detailed histopathological assessment of H&E-stained sections to evaluate tissue-specific inflammatory changes in *C. braakii*-infected NMRs. All sections were evaluated by three independent board-certified pathologists with expertise spanning human gastrointestinal and rodent pathology. Histological analysis revealed characteristic inflammatory patterns, including leucocyte infiltration in the mucosa (Figure 4A), submucosa (Figure 4B), and transmural patches (Figure 4C). Semi-quantitative evaluation graded inflammation severity as mild, moderate, and severe based on the extent and localisation of leucocyte infiltration (Figure 4D, left). Based on mean scores from three pathologists, the cohort showed a spectrum of inflammation severity (Figure 4D, right). One animal (ID 6) demonstrated mild inflammation (mean Score 1.3), characterised by an increased presence of inflammatory cells in the mucosa compared to healthy controls. Five infected NMRs exhibited moderate inflammation (Score 2), defined by moderate leucocyte density localised to the mucosa and the submucosa. One NMR showed severe inflammation (mean Score 2.8), which was characterised by leucocyte presence extending into the muscularis propria and forming transmural infiltrates (Figure 4D, right).

Probiotic treatment ameliorates bacteria-induced colitis and promotes systemic health in NMRs

Two weeks after the second infected cohort of NMRs ($n = 7$) was removed from their colony for disease characterisation, a third group ($n = 10$; five females and five males) developed symptoms, including fatigue and diarrhoea, and was immediately isolated to prevent any further infectious transmission via coprophagy. Confirmation of *C. braakii* colonisation in the livers and Gram-negative immunopositivity in colons and caecum of early euthanised animals led to the hypothesis that probiotic intervention might ameliorate bacterially induced colitis, as previously observed in *C. rodentium*-infected mice [69]. Accordingly, we treated colitic NMRs with a seven-strain probiotic cocktail (Protexin) containing *Lactobacillus plantarum*, *L. delbrueckii* subsp. *bulgaricus*, *L. acidophilus*, *L. rhamnosus*, *Bifidobacterium bifidum*, *Streptococcus salivarius* subsp. *thermophilus*, and *Enterococcus faecium*. An overview of the sporadic outbreak timeline, cohort allocations, and experimental interventions is provided in supplementary material, Figure S1.

Affected animals were administered Protexin at varying disease stages (mild, moderate, and severe), determined by the time since first symptom onset. As such, the infected NMRs were subdivided into three treatment groups, which included NMRs displaying symptoms for 2.5 weeks ($n = 3$), 6.5 weeks ($n = 3$), and 11 weeks ($n = 4$). We monitored weight gain and stool appearance. Weight recovery correlated with disease severity at the start of treatment. More specifically, the mild and moderate groups regained 98% of their initial body mass within 3–4 weeks, whereas the severe colitis group took approximately 20 weeks to reach 80% of their initial body weight (Figure 5A,B). This rate and completeness

Figure 2. NMRs are susceptible to *C. braakii* infection. (A) (Left) Peripheral blood smear with Wright–Giemsa stain shows both extracellular (black arrow) and intracellular rod-shaped bacteria (blue arrow) and (right) bacteria of coccoid morphology (black arrow). Scale bars, 5 µm. (B) Bar chart showing percentage of different immune cell populations over total leucocyte counts in peripheral blood of healthy solitary [$n = 4$; one female (F), three male (M); all 36 months] and infected ($n = 5$; four F, one M; median age: 30 months, interquartile range (IQR): 23–34) NMRs. *P* values generated using Mann–Whitney *U* test (two-tailed) are indicated. (C) Photomicrographs showing caecum and colonic tissue sections of infected NMRs stained with haematoxylin and anti-lipopolysaccharide antibody. Scale bars, 100 µm. (D) Photomicrographs showing caecum and colonic tissue sections of infected NMRs stained with haematoxylin and anti-lipoteichoic acid antibody. Scale bars, 100 µm.

of body weight recovery was most strongly associated with baseline disease severity. Animals with mild and moderate disease regained body mass rapidly, while those with severe colitis exhibited slower recovery, plausibly due to reduced food intake during more pronounced illness (Figure 5B). Interestingly, healthy

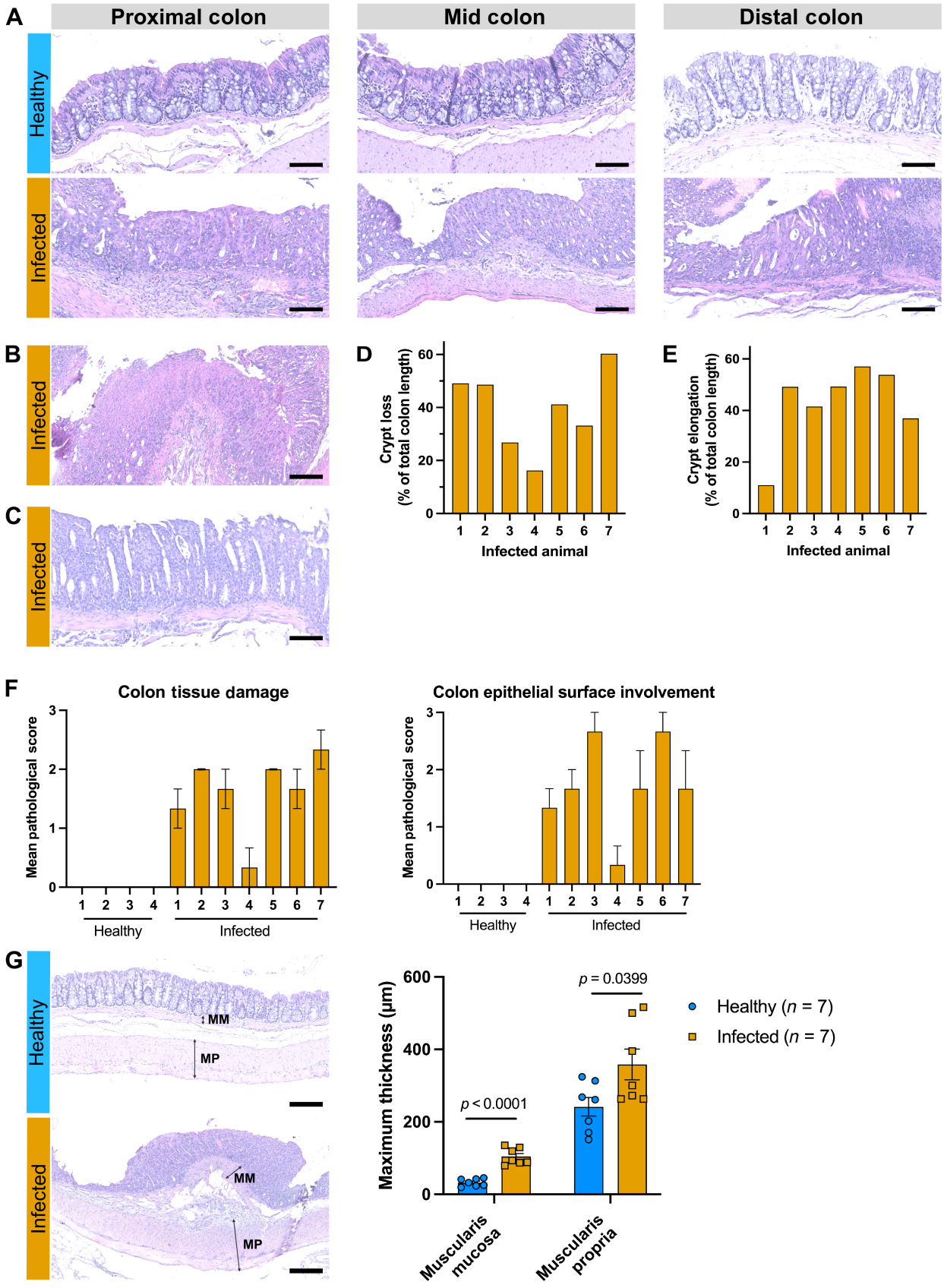

Figure 3 Legend on next page.

NMRs fed Protexin for 32 weeks gained 23% more weight than untreated healthy NMRs, suggesting a growth-promoting or metabolic effect from the probiotic supplement (Figure 5B).

Improvement in stool consistency was also observed. NMRs with mild disease showed changes in their stool score from Score 2 to Score 0 within 3 weeks of probiotic administration (Figure 5C). NMRs with moderate and severe colitic disease took 6 weeks of treatment to reach normal stool consistency (Figure 5C). In addition to these external measurements of disease remission, we also euthanised NMRs from the mild ($n = 1$), moderate ($n = 1$), and severe ($n = 1$) colitis group after 48 weeks of Protexin treatment for histomorphological analysis. The length of the colon, which contracts during colitis, was similar between treated and healthy control animals ($n = 6$) (Figure 5D). Probiotic treatment restored normal crypt architecture and significantly reduced the thickening of the muscularis mucosa and muscularis propria observed in infected NMRs (Figure 5E). Quantitative analysis confirmed these observations, revealing an approximately four-fold reduction (~75%) in muscularis mucosa thickness and a two-fold reduction (~50%) in muscularis propria thickness compared to untreated infected NMRs (Figure 5E, right). Furthermore, the remaining treated NMRs were monitored for over 2 years after treatment, during which they remained healthy, viable for breeding and successfully established new colonies, which demonstrated sustained disease remission and fully restored fitness.

Probiotic-mediated recovery of goblet cells and proliferation dynamics in colitic NMRs

Previous studies of infectious colitis demonstrated that epithelial barrier disruption, including goblet cell depletion and crypt cell hyperproliferation, commonly

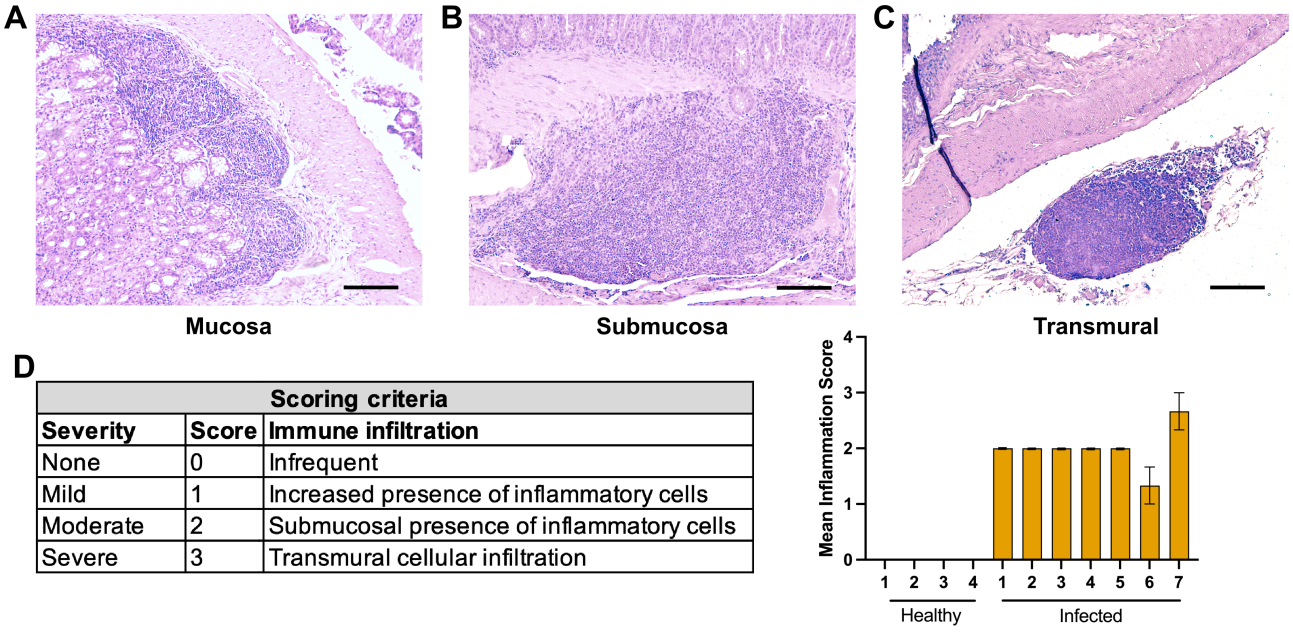

Scoring criteria		
Severity	**Score**	**Immune infiltration**
None	0	Infrequent
Mild	1	Increased presence of inflammatory cells
Moderate	2	Submucosal presence of inflammatory cells
Severe	3	Transmural cellular infiltration

Figure 4. Colonic inflammation in *C. braakii*-infected NMRs. (A–C) H&E-stained microscopic images showing extensive colonic inflammation in *C. braakii*-infected NMRs in mucosal (A), submucosal (B), andtransmural (C) patches. Scale bars, 100 μm. (D) (Left) Table highlighting scoring scheme used for semi-quantitative analysis of inflammation severity. (Right) Bar chart depicting mean pathological score of inflammation in infected NMRs.

Figure 3. Histomorphology of colon in *C. braakii*-infected NMRs. (A) (Top) Representative H&E-stained microscopic images showing colonic tissue (proximal, mid, and distal) of healthy NMRs (scale bars, 100 μm). (Bottom) H&E-stained images showing colons of *C. braakii*-infected NMRs. (B and C) H&E-stained microscopic images showing aberrant epithelial histomorphology in infected NMRs consisting of crypt loss (B) (scale bar, 200 μm) and crypt elongation (C) (scale bar, 100 μm). (D and E) Bar charts showing proportion of colonic tissue exhibiting crypt loss (D) or elongation (E) in infected NMRs [$n = 7$, five females (F), two males (M), median age: 33 months, interquartile range (IQR): 23–42]. Lengths were measured using ImageJ software on microscopic images acquired at 2× magnification. (F) Bar charts depicting mean pathological scores based on (left) overall colonic tissue damage and (right) epithelial surface involvement obtained from the histological assessment of infected NMRs by three independent pathologists using the scoring criteria highlighted in the table (supplementary material, Figure S4). (G) (Left) Photomicrographs demarcating muscularis mucosa (MM) and muscularis propria (MP) in healthy and infected NMR colonic tissue (scale bars, 200 μm). (Right) Quantification of MM and MP thickness in colonic tissue from healthy ($n = 7$; four F, three M; all aged 36 months) and infected ($n = 7$; five F, two M; median age: 33 months, interquartile range: 23–42) NMRs. Bar charts showing peak hypertrophic response by measuring the maximum thickness (μm) for each muscle layer. Three separate measurements were taken per animal, and the mean (± SEM) was calculated. *P* values are shown.

results from pathogen-induced inflammation [69,70]. Probiotics are known to promote epithelial repair, restore microbial balance, and strengthen the intestinal barrier [71]. Given this evidence, we next assessed the effect of probiotic administration on mucosal architecture in colitic NMRs, focusing on these cellular features. Our digital analysis of Alcian blue-stained sections revealed striking alterations in goblet cell morphology. Infected NMRs exhibited a five-fold reduction in mean goblet cell area (~20.7 μm^2) compared to healthy controls (~109.3 μm^2), indicating significant cellular atrophy and depletion of mucin production. Remarkably, we found that probiotic treatment not only reversed this pathology but enhanced goblet cell morphology,

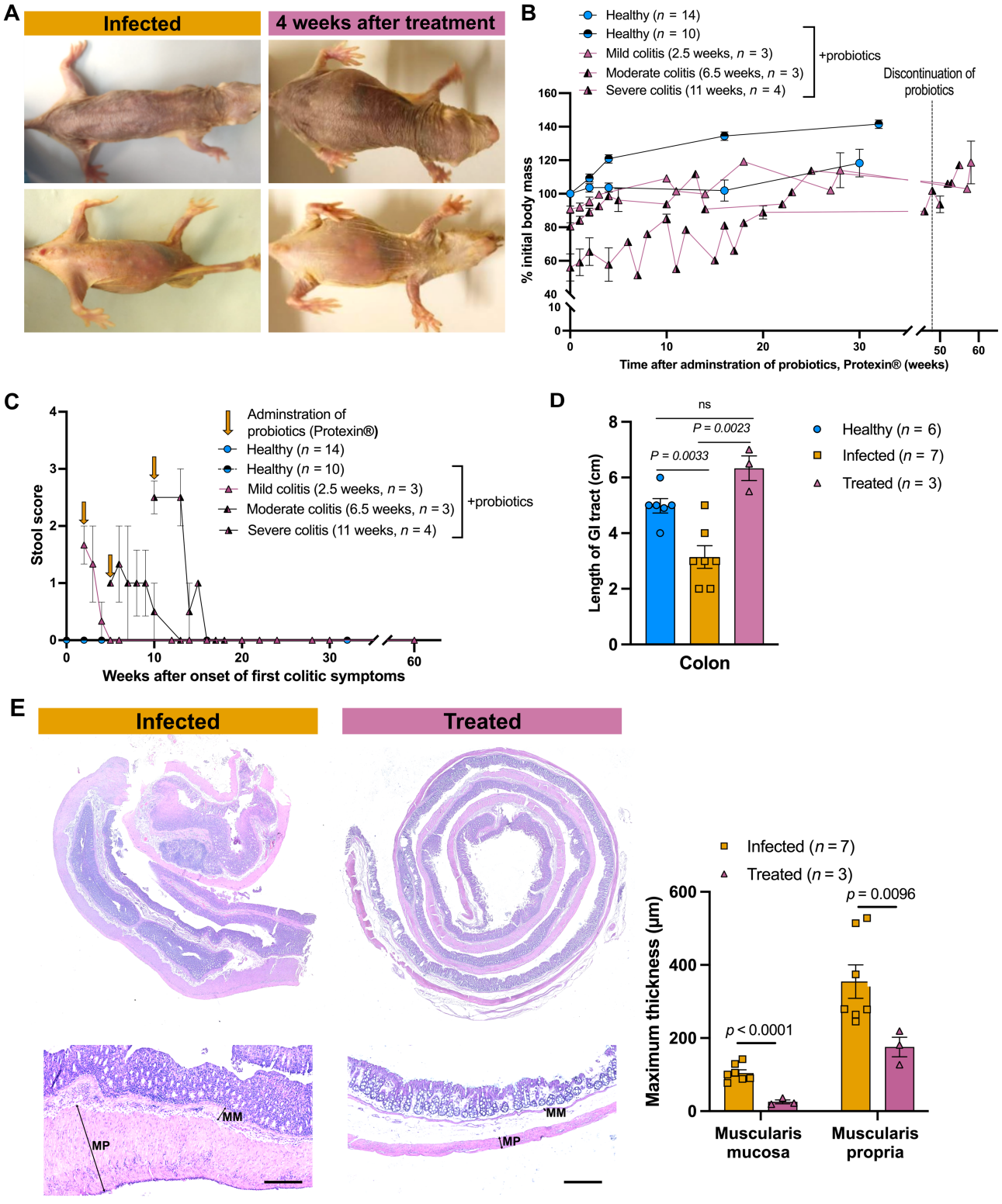

Figure 5 Legend on next page.

achieving a 7.5-fold increase in surface area (~154.6 μm^2) relative to infected animals, which corresponded to a 1.4-fold increase over healthy baseline levels (Figure 6A).

We next performed immunohistochemical staining for Ki67. Our quantitative analysis revealed profound hyperproliferation in the epithelium of infected NMRs, with increases of 125% ($p < 0.0001$; 95% CI: 7.81–10.34), 112% ($p < 0.0001$; 95% CI: 7.62–9.94), and 83% ($p < 0.0001$; 95% CI: 6.25–8.80) in the Ki67 positivity of cryptal cells in the proximal, mid, and distal colon, respectively, compared to healthy controls (Figure 6B). Probiotic intervention dramatically reduced crypt cell proliferation rates across all colonic regions (proximal: 95% CI: −8.39 to −5.91; mid: 95% CI: −7.59 to −5.11; distal: 95% CI: −11.26 to −8.94; all $p < 0.0001$ versus infected). In summary, probiotic treatment comprehensively reversed the infectious colitis phenotype in NMRs by simultaneously restoring goblet cell morphology and normalising epithelial proliferation to promote mucosal recovery.

Discussion

NMRs have emerged as an exciting model for anti-ageing studies due to their exceptionally long lifespan, high fecundity, and low burden of age-related diseases [29,72]. Much research has focused on elucidating evolutionary pressures and biological mechanisms driving these unique traits in NMRs that ensure long-term tissue maintenance and disease resistance. However, a few reports on spontaneous and experimentally induced pathologies have highlighted specific weaknesses in the otherwise robust biology of NMRs and offer a unique opportunity to use these fascinating mammals to understand mechanisms underlying human diseases. For example, NMRs are highly susceptible to viral infections like HSV1 [51] and coronaviruses [52], which appears to be due to relaxed viral selection pressures on NMRs as they have minimal exposure to airborne viruses while inhabiting sealed subterranean burrows. Further insight into common pathologies in NMRs has come from necropsy data in research colonies and zoo populations that have revealed the prevalence of renal tubular mineralisation, hepatic haemosiderosis, bite wounds, and chronic progressive nephropathy [27,73].

The spontaneous disease outbreak in our NMR colonies adds to the rarely reported disease processes in NMRs and highlights the critical role of intestinal homeostasis in maintaining the overall health of long-lived NMRs. Our findings serendipitously demonstrate a new role for NMRs as a highly relevant and much-needed research tool for studying the multisystem interactions of pathogenic gut bacteria in inducing local and systemic inflammation that contributes to the development of inflammatory diseases [74] and life-threatening sepsis [75]. In the results presented here, we show that colonisation of Gram-negative bacteria in the submucosal layers in the caecum and colon resulted in clinical and histopathological features in NMRs that closely resemble the hallmark characteristics of mouse and human colitis [53,54]. In addition to presenting with weight loss, severe dehydration, perianal ulceration, and bloody diarrhoea, histomorphological analyses of the intestinal tract showed distortions in the mucosal architecture and extensive epithelial atypia. These included ulcerations, thickening of the muscularis propria, loss of surface epithelium, hyperproliferation, and crypt abnormalities. We also observed goblet cell loss in the colonic epithelium, which would reduce barrier maintenance and allow increased exposure to luminal bacteria. In future studies, it will be interesting to study how goblet cell depletion is mediated by enteric infections and how this impacts colitis progression and/or host defence. Interestingly, we previously reported that healthy NMRs had a higher abundance of goblet cells, higher gene expression levels of mucins, and a thicker mucin layer in the colon compared to mice, and we also showed that NMRs had a higher resistance to dextran sulphate sodium-induced colitis [36]. Another recent study showed reduced gut permeability in NMRs by measuring intestinal anion secretion induced by serotonin, bradykinin, histamine, and capsaicin [37]. These observations underscore the remarkable protective baseline of the NMR gut epithelium. Despite these indications of a robust

Figure 5. Probiotic treatment ameliorates bacterially induced colitis and promotes systemic health in NMRs. (A) Representative photographs showing gross morphological changes in NMRs after 4 weeks of treatment with seven-strain probiotic formulation (Protexin). (B) Line graph showing mean body mass change (± SEM) over time in NMR cohorts: untreated healthy NMRs ($n = 14$), Protexin-treated healthy ($n = 10$), and Protexin-treated colitic NMRs ($n = 10$) monitored over time. Colitic NMRs are subdivided by disease severity at treatment initiation: mild [$n = 3$; two females (F), one male (M); median age: 30 months, interquartile range (IQR): 24–34; symptomatic for 2.5 weeks], moderate ($n = 3$; one F, two M; median age: 38 months, IQR: 22–42; symptomatic for 6.5 weeks), and severe ($n = 4$; two F, two M; median age: 33 months, IQR: 20–42; symptomatic for 11 weeks). Healthy controls include colony-dwelling untreated NMRs ($n = 14$; seven F, seven M; median age: 44 months, IQR: 23–57) and Protexin-treated healthy NMRs ($n = 10$; five F, five M; median age: 33 months, IQR: 22–42). (C) Line graph showing changes in mean stool score (± SEM) over time for cohorts described in panel (B). (D) Bar chart showing mean length (± SEM) of colons in healthy untreated ($n = 6$; three F, three M; median age: 36 months, IQR: 36–38), infected ($n = 7$; five F, two M; median age: 33 months, IQR: 23–42), and probiotic-treated NMRs after 48 weeks ($n = 3$; two F, one M; median age: 24 months, IQR: 22–33). (E) Histomorphological analysis. (Top) Representative H&E-stained Swiss-roll preparations of entire colonic tissue from infected and probiotic-treated NMRs. (Bottom) Higher-magnification images comparing muscle layers; black lines demarcate muscularis mucosa (MM) and muscularis propria (MP) (scale bars, 200 μm). (Right) Bar charts showing differences in thickness of MM and MP in infected ($n = 7$) and treated ($n = 3$) NMRs. Data represent mean (± SEM) of three measurements per animal at sites of maximum thickness (μm). *P* values are indicated (Student's *t*-test, two-tailed, unpaired, unequal variance).

intestinal barrier in NMRs against experimentally induced irritants, we now show that natural infection by pathogenic bacteria can break down the epithelial integrity in the colon of these animals and induce severe colitis. This highlights both the virulence of the pathogen and the value of the NMR as a model for dissecting mechanisms of mucosal barrier breach and host–pathogen interactions.

Dysregulation of immune responses in the intestinal mucosa is central to the pathogenesis of human

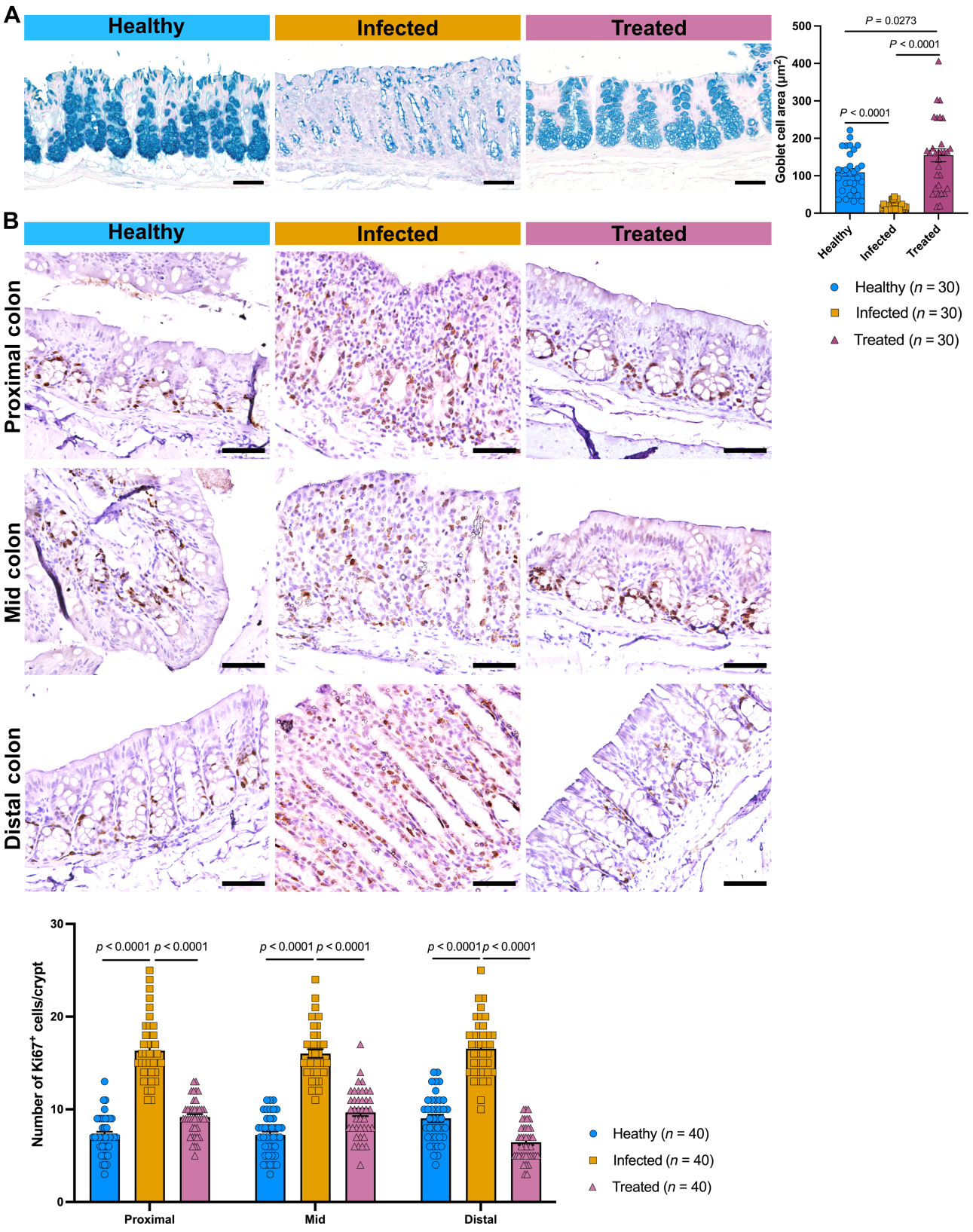

Figure 6 Legend on next page.

inflammatory diseases and other forms of infectious colitis [76–78]. Indeed, bacterially infected NMRs showed moderate to severe leucocyte infiltration specifically in the colonic mucosa and submucosa. We were unable to characterise specific immune cell infiltrates in the intestinal tissue of these animals due to the incompatibility of commercially available antibodies to cross-react with NMRs. Recent work has begun to screen for antibodies that exhibit cross-reactivity to certain NMR cell-surface markers [79], but this panel remains very limited and does not yet include practical reagents for the full suite of colitis-relevant inflammatory or lymphocyte markers (such as CD4, CD8, CD68, or FOXP3). As such, standard immunophenotyping approaches remain technically challenging in NMRs at present, and all tissue scoring in our study was performed by three independent pathologists. Future work using sequencing technology will need to be employed to fully characterise the immune responses associated with bacterially induced colonic inflammation in NMRs. In addition to colonic inflammation, assessing the peripheral blood of infected NMRs highlighted a robust innate immune response systemically. More specifically, there was a significant increase in immature neutrophils and monocytes and a concomitant decrease in mature neutrophils. These observations are in line with emergency myelopoiesis seen in septic mice [80] or amplified granulopoiesis seen in human septic patients [60]. Interestingly, NMRs lack canonical NK cells [45], in contrast to other rodent models, such as mice, where NK cells are critical in controlling *Citrobacter* infection and limiting bacterial expansion and systemic spread via cytotoxicity and cytokine production [81]. Instead, NMRs possess a uniquely myeloid-biased immune system with elevated granulocyte and macrophage activity [48,82]. The observed innate immune response in our study, particularly emergency myelopoiesis and increased immature neutrophils and monocytes, may reflect these alternative immune cell populations compensating for the absence of NK cells. The implications of this adaptation, especially in terms of susceptibility or resilience to enteric bacterial pathogens, highlight the value of this species for studying alternative immune strategies that have evolved in long-lived mammals.

Interestingly, we detected both coccoid and rod-shaped bacteria in the blood and a heavy outgrowth of *C. braakii* in the livers of morbid NMRs. *C. braakii* is a Gram-negative, facultative anaerobe of the *C. freundii* complex [83], which has been found in clinical gastrointestinal specimens and is thought to be an opportunistic microorganism [84,85]. Interestingly, in mice, another member of this enterobacteria family, *C. rodentium*, has been shown to induce colitis, sharing pathogenicity with human enteropathogenic *E. coli* and enterohaemorrhagic *E. coli* [69,86]. These bacteria, referred to as attaching and effacing (A/E) bacteria, share the pathogenic mechanism of colonising the intestinal mucosa by attaching to the intestinal epithelium and effacing the epithelial brush border [87–89]. Our comparative analysis revealing a high sequence homology of *C. braakii* with *C. rodentium* and *E. coli* suggests related enteropathogenic mechanisms and related pathophysiology across species. While our findings indicate a significant role for *C. braakii*, as evidenced by its consistent isolation and heavy growth in culture from multiple organs, it is important to note that bacterial load was assessed semi-quantitatively rather than by precise CFU enumeration. This approach, while standard for clinical diagnostics, limits the granularity of our bacterial burden analysis. Future studies employing quantitative culture techniques would provide more precise data on the relationship between bacterial numbers and disease severity. Although *C. braakii* was not isolated from gut tissue, the combination of clinical presentation, histopathological evidence of colitis, LPS immunostaining in the colon, and consistent isolation of *C. braakii* from liver and lung strongly support this species as the causative pathogen responsible for both colitis and systemic disease in this outbreak. Taken together, we conclude that the disease process in NMRs initiated in the lower gastrointestinal tract, with *C. braakii* translocating from the caecal and colonic mucosa to the systemic circulation, resulting in liver colonisation and sepsis.

Members of the Enterobacteriaceae family, namely *C. rodentium* and *Salmonella*, have elucidated the role of enteropathogenic infections and host inflammation in disrupting colonic microbial community that provides a competitive growth advantage to the enteric pathogen and enhances its virulence [90–92]. One possible way to restore microbial balance is the use of probiotic microorganisms that have been shown to promote a healthy gut microbiota and a healthy immune system [93–96]. For example, *Bifidobacterium* spp. and *Lactobacillus* spp. probiotic treatment have been shown to reduce mortality, promote intestinal mucus secretion, and reduce inflammation in zebrafish [97] and mice

Figure 6. Probiotic-mediated recovery of goblet cells and proliferation dynamics in colitic NMRs. (A) Goblet cell analysis. (Left) Representative Alcian Blue-stained images of colonic goblet cells in healthy, infected, and probiotic-treated NMRs (scale bars, 50 μm). (Right) Bar chart quantifying mean (± SEM) goblet cell area (μm^2) in healthy ($n = 5$; two female (F), three male (M); all aged 36 months), infected NMRs ($n = 7$; five F, two M; median age: 33 months, interquartile range (IQR): 23–42), and probiotic-treated NMRs ($n = 3$; two F, one M; median age: 24 months, IQR: 22–33). For each animal, at least 30 goblet cells were measured across three randomly selected areas in the colon. *P* values are indicated on the graph (Student's *t*-test, two-tailed, unpaired, unequal variance). (B) Crypt cell proliferation analysis. (Top) Photomicrographs of Ki67 immunostaining in proximal, mid, and distal colons of healthy, infected, and probiotic-treated NMRs (scale bars, 50 μm). (Bottom) Bar chart showing mean number (± SEM) of Ki67-positive cells in proximal, mid, and distal regions of colons of healthy ($n = 2$; one F, one M), infected ($n = 2$; two F), and probiotic-treated ($n = 2$; one F, one M) NMRs. Forty crypts in each region of the colon were counted per animal. *P* values are indicated on graph (Student's *t*-test, two-tailed, unpaired, unequal variance).

[98,99]. Similarly, VSL#3, which contains eight bacterial strains, including *Lactobacillus, Bifidobacterium*, and *Streptococcus* subspecies, has also been shown to alter intestinal permeability in *Muc2*-deficient mice and exert a beneficial effect independent of an intact mucus layer [100]. Even in humans, the addition of probiotics like VSL#3 to the conventional treatment of ulcerative colitis patients results in more efficacious remission [101–103]. Taking inspiration from these studies, we treated NMRs infected with *C. braakii* with a commercially available seven-strain probiotic (Protexin). Protexin contains *L. plantarum, L. delbrueckii* subsp. *bulgaricus, L. acidophilus, L. rhamnosus, Bifidobacterium bifidum, Streptococcus salivarius* subsp. *Thermophilus*, and *Enterococcus faecium*. Indeed, the use of Protexin had a strong therapeutic effect and reversed the disease phenotype in *C. braakii*-infected NMRs. We observed restoration of the mucosal architecture, replenishment of colonic goblet cells, and reduction in the proliferative index of cryptal cells that were comparable to levels seen in uninfected, healthy NMRs. A limitation of our probiotic intervention is the potential variability in daily dosage due to the dietary administration, which was chosen to minimise stress in symptomatic animals. Consequently, we cannot rule out the possibility that reduced food consumption in severely ill animals contributed to their slower recovery by lowering their effective probiotic intake. Future studies will explore other dosing protocols to further refine the dosage and assess the full therapeutic effect of probiotics in highly severe cases. While the role of individual subspecies in alleviating the effects of infectious colitis in NMRs remains to be determined, our results show how ecological rebalance in the intestinal flora by probiotics has a profound effect in promoting intestinal homeostasis in these animals.

In summary, our findings highlight how intestinal health is critical for maintaining the overall health of long-lived NMRs, and any overgrowth of a bacterial pathogen can lead to intestinal epithelial damage and pro-inflammatory responses, which culminate in bacterially induced colitis and sepsis. Therefore, we propose the NMR as a valuable model for studying specific pathogen-related colitis where new models are increasingly required to address the multifactorial aetiology and clinical heterogeneity caused by common bacteria such as *Campylobacter jejuni, Salmonella, Shigella, E. coli, Yersinia enterocolitica, Clostridioides difficile*, and *Mycobacterium tuberculosis* [104]. Furthermore, the profound efficacy of probiotics in reversing the pathophysiology of infectious colitis underscores the potential of the NMR model for developing and testing microbiome-focused therapeutics against enteropathogenic infections and associated pro-inflammatory diseases of the gut.

Acknowledgements

Special thanks go to Dr Yolandi Rautenbach, Carien Muller, and the rest of the Clinical Pathology team at the Department of Companion Animal Clinical Studies, Faculty of Veterinary Science, University of Pretoria, for conducting the haematological analysis for this project. We also extend our gratitude to Mr Erick Kapp from the Bacteriology Laboratory, Department of Veterinary Tropical Diseases, Faculty of Veterinary Science, University of Pretoria, for performing the bacteriology tests. We are also grateful to Professor Nan Gao (Rutgers, The State University of New Jersey), Dr Sandrine Ménard (Institut de Recherche en Santé Digestive, Université de Toulouse), and Sir Walter Bodmer (University of Oxford) for their comments on the manuscript. This research was supported financially by the South African Research Chair of Mammal Behavioural Ecology and Physiology from the Department of Science and Technology-National Research Foundation (DST-NRF) (GUN 64756, NCB) and the NIHR-BRC funding (JEE and SI). The views expressed are those of the authors and not necessarily those of the National Health Service, the NIHR or the Department of Health.

Author contributions statement

NMRs and ethics for *in vivo* work were acquired by NCB and DWH. Animal experiments were conducted by DWH. Histological staining, microscopy, phylogenetic and statistical analyses were performed by ASN, AZ and LP. Histopathological scoring was performed by PG, RG and PG. Post-mortem examination was done by NO. Tissue processing was done by SM. Intellectual input was provided by DWH, CB, NK, JEE, IPMT and NCB. Funding was acquired by JEE, NCB and SI. The manuscript was written by SI with feedback from all other authors. All authors approved the submitted version of the manuscript.

Data availability statement

The data that support the findings of this study are available from the corresponding author upon reasonable request.

References

1. Herzog MK, Cazzaniga M, Peters A, *et al*. Mouse models for bacterial enteropathogen infections: insights into the role of colonization resistance. *Gut Microbes* 2023; **15:** 2172667.
2. Boirivant M, Fuss IJ, Chu A, *et al*. Oxazolone colitis: a murine model of T helper cell type 2 colitis treatable with antibodies to interleukin 4. *J Exp Med* 1998; **188:** 1929–1939.
3. Kuhn R, Lohler J, Rennick D, *et al*. Interleukin-10-deficient mice develop chronic enterocolitis. *Cell* 1993; **75:** 263–274.
4. Nenci A, Becker C, Wullaert A, *et al*. Epithelial NEMO links innate immunity to chronic intestinal inflammation. *Nature* 2007; **446:** 557–561.
5. Neurath MF, Fuss I, Kelsall BL, *et al*. Antibodies to interleukin 12 abrogate established experimental colitis in mice. *J Exp Med* 1995; **182:** 1281–1290.

6. Okayasu I, Hatakeyama S, Yamada M, *et al*. A novel method in the induction of reliable experimental acute and chronic ulcerative colitis in mice. *Gastroenterology* 1990; **98:** 694–702.
7. Powrie F, Leach MW, Mauze S, *et al*. Phenotypically distinct subsets of CD4+ T cells induce or protect from chronic intestinal inflammation in C. B-17 scid mice. *Int Immunol* 1993; **5:** 1461–1471.
8. Mombaerts P, Mizoguchi E, Grusby MJ, *et al*. Spontaneous development of inflammatory bowel disease in T cell receptor mutant mice. *Cell* 1993; **75:** 274–282.
9. Sadlack B, Merz H, Schorle H, *et al*. Ulcerative colitis-like disease in mice with a disrupted interleukin-2 gene. *Cell* 1993; **75:** 253–261.
10. Chen X, Katchar K, Goldsmith JD, *et al*. A mouse model of Clostridium difficile-associated disease. *Gastroenterology* 2008; **135:** 1984–1992.
11. Collignon A. Methods for working with the mouse model. *Methods Mol Biol* 2010; **646:** 229–237.
12. Ehrhardt K, Grassl GA. Mouse model to study salmonella-induced colitis. *Methods Mol Biol* 2022; **2427:** 201–213.
13. Uhlig HH, McKenzie BS, Hue S, *et al*. Differential activity of IL-12 and IL-23 in mucosal and systemic innate immune pathology. *Immunity* 2006; **25:** 309–318.
14. Gerlach K, Hwang Y, Nikolaev A, *et al*. TH9 cells that express the transcription factor PU.1 drive T cell-mediated colitis via IL-9 receptor signaling in intestinal epithelial cells. *Nat Immunol* 2014; **15:** 676–686.
15. Krug SM, Bojarski C, Fromm A, *et al*. Tricellulin is regulated via interleukin-13-receptor alpha2, affects macromolecule uptake, and is decreased in ulcerative colitis. *Mucosal Immunol* 2018; **11:** 345–356.
16. Scheibe K, Kersten C, Schmied A, *et al*. Inhibiting interleukin 36 receptor signaling reduces fibrosis in mice with chronic intestinal inflammation. *Gastroenterology* 2019; **156:** 1082–1097 e1011.
17. Mestas J, Hughes CC. Of mice and not men: differences between mouse and human immunology. *J Immunol* 2004; **172:** 2731–2738.
18. Ariffin JK, Sweet MJ. Differences in the repertoire, regulation and function of toll-like receptors and inflammasome-forming nod-like receptors between human and mouse. *Curr Opin Microbiol* 2013; **16:** 303–310.
19. Shay T, Jojic V, Zuk O, *et al*. Conservation and divergence in the transcriptional programs of the human and mouse immune systems. *Proc Natl Acad Sci U S A* 2013; **110:** 2946–2951.
20. Beura LK, Hamilton SE, Bi K, *et al*. Normalizing the environment recapitulates adult human immune traits in laboratory mice. *Nature* 2016; **532:** 512–516.
21. Reese TA, Bi K, Kambal A, *et al*. Sequential infection with common pathogens promotes human-like immune gene expression and altered vaccine response. *Cell Host Microbe* 2016; **19:** 713–719.
22. Atarashi K, Tanoue T, Shima T, *et al*. Induction of colonic regulatory T cells by indigenous clostridium species. *Science* 2011; **331:** 337–341.
23. Abolins S, King EC, Lazarou L, *et al*. The comparative immunology of wild and laboratory mice, Mus musculus domesticus. *Nat Commun* 2017; **8:** 14811.
24. Japp AS, Hoffmann K, Schlickeiser S, *et al*. Wild immunology assessed by multidimensional mass cytometry. *Cytometry A* 2017; **91:** 85–95.
25. Chung H, Pamp SJ, Hill JA, *et al*. Gut immune maturation depends on colonization with a host-specific microbiota. *Cell* 2012; **149:** 1578–1593.
26. Buffenstein R, Jarvis JU. The naked mole rat--a new record for the oldest living rodent. *Sci Aging Knowl Environ* 2002; **2002:** pe7.
27. Delaney MA, Nagy L, Kinsel MJ, *et al*. Spontaneous histologic lesions of the adult naked mole rat (Heterocephalus glaber): a retrospective survey of lesions in a zoo population. *Vet Pathol* 2013; **50:** 607–621.
28. Buffenstein R. Negligible senescence in the longest living rodent, the naked mole-rat: insights from a successfully aging species. *J Comp Physiol B* 2008; **178:** 439–445.
29. Buffenstein R. The naked mole-rat: a new long-living model for human aging research. *J Gerontol A Biol Sci Med Sci* 2005; **60:** 1369–1377.
30. Delaney MA, Ward JM, Walsh TF, *et al*. Initial case reports of cancer in naked mole-rats (Heterocephalus glaber). *Vet Pathol* 2016; **53:** 691–696.
31. Taylor KR, Milone NA, Rodriguez CE. Four cases of spontaneous neoplasia in the naked mole-rat (Heterocephalus glaber), a putative cancer-resistant species. *J Gerontol A Biol Sci Med Sci* 2017; **72:** 38–43.
32. Cole JE, Steeil JC, Sarro SJ, *et al*. Chordoma of the sacrum of an adult naked mole-rat. *J Vet Diagn Invest* 2020; **32:** 132–135.
33. Grimes KM, Reddy AK, Lindsey ML, *et al*. And the beat goes on: maintained cardiovascular function during aging in the longest-lived rodent, the naked mole-rat. *Am J Physiol Heart Circ Physiol* 2014; **307:** H284–H291.
34. O'Connor TP, Lee A, Jarvis JU, *et al*. Prolonged longevity in naked mole-rats: age-related changes in metabolism, body composition and gastrointestinal function. *Comp Biochem Physiol A Mol Integr Physiol* 2002; **133:** 835–842.
35. Gustafsson JK, Ermund A, Johansson ME, *et al*. An ex vivo method for studying mucus formation, properties, and thickness in human colonic biopsies and mouse small and large intestinal explants. *Am J Physiol Gastrointest Liver Physiol* 2012; **302:** G430–G438.
36. Montazid S, Bandyopadhyay S, Hart DW, *et al*. Adult stem cell activity in naked mole rats for long-term tissue maintenance. *Nat Commun* 2023; **14:** 8484.
37. Aguilera-Lizarraga J, Ritoux A, Bulmer DC, *et al*. Intestinal barrier function in the naked mole-rat: an emergent model for gastrointestinal insights. *Am J Physiol Gastrointest Liver Physiol* 2024; **327:** G188–G201.
38. Chua KO, Fatima I, Lau YY, *et al*. Bacterial microbiome of faecal samples of naked mole-rat collected from the toilet chamber. *BMC Res Notes* 2022; **15:** 107.
39. Debebe T, Biagi E, Soverini M, *et al*. Unraveling the gut microbiome of the long-lived naked mole-rat. *Sci Rep* 2017; **7:** 9590.
40. Cong W, Xing J, Feng Y, *et al*. The microbiota in the intestinal and respiratory tracts of naked mole-rats revealed by high-throughput sequencing. *BMC Microbiol* 2018; **18:** 89.
41. Debebe T, Holtze S, Morhart M, *et al*. Analysis of cultivable microbiota and diet intake pattern of the long-lived naked mole-rat. *Gut Pathog* 2016; **8:** 25.
42. Schnorr SL, Candela M, Rampelli S, *et al*. Gut microbiome of the Hadza hunter-gatherers. *Nat Commun* 2014; **5:** 3654.
43. Smits SA, Leach J, Sonnenburg ED, *et al*. Seasonal cycling in the gut microbiome of the Hadza hunter-gatherers of Tanzania. *Science* 2017; **357:** 802–806.
44. Biagi E, Franceschi C, Rampelli S, *et al*. Gut microbiota and extreme longevity. *Curr Biol* 2016; **26:** 1480–1485.
45. Hilton HG, Rubinstein ND, Janki P, *et al*. Single-cell transcriptomics of the naked mole-rat reveals unexpected features of mammalian immunity. *PLoS Biol* 2019; **17:** e3000528.
46. Emmrich S, Trapp A, Tolibzoda Zakusilo F, *et al*. Characterization of naked mole-rat hematopoiesis reveals unique stem and progenitor cell patterns and neotenic traits. *EMBO J* 2022; **41:** e109694.
47. Begay V, Cirovic B, Barker AJ, *et al*. Immune competence and spleen size scale with colony status in the naked mole-rat. *Open Biol* 2022; **12:** 210292.
48. Gorshkova EA, Gubernatorova EO, Dvorianinova EM, *et al*. Macrophages from naked mole-rat possess distinct immunometabolic signatures upon polarization. *Front Immunol* 2023; **14:** 1172467.

49. Cheng J, Yuan Z, Yang W, *et al*. Comparative study of macrophages in naked mole rats and ICR mice. *Oncotarget* 2017; **8:** 96924–96934.
50. Wada H, Shibata Y, Abe Y, *et al*. Flow cytometric identification and cell-line establishment of macrophages in naked mole-rats. *Sci Rep* 2019; **9:** 17981.
51. Artwohl J, Ball-Kell S, Valyi-Nagy T, *et al*. Extreme susceptibility of African naked mole rats (Heterocephalus glaber) to experimental infection with herpes simplex virus type 1. *Comp Med* 2009; **59:** 83–90.
52. Ross-Gillespie A, O'Riain MJ, Keller LF. Viral epizootic reveals inbreeding depression in a habitually inbreeding mammal. *Evolution* 2007; **61:** 2268–2273.
53. Erben U, Loddenkemper C, Doerfel K, *et al*. A guide to histomorphological evaluation of intestinal inflammation in mouse models. *Int J Clin Exp Pathol* 2014; **7:** 4557–4576.
54. DeRoche TC, Xiao SY, Liu X. Histological evaluation in ulcerative colitis. *Gastroenterol Rep (Oxf)* 2014; **2:** 178–192.
55. Hart DW, Bennett NC, Oosthuizen MK, *et al*. Energetics and water flux in the subterranean rodent family Bathyergidae. *Front Ecol Evol* 2022; **10:** 867350.
56. Edgar RC. MUSCLE: multiple sequence alignment with high accuracy and high throughput. *Nucleic Acids Res* 2004; **32:** 1792–1797.
57. Takizawa H, Boettcher S, Manz MG. Demand-adapted regulation of early hematopoiesis in infection and inflammation. *Blood* 2012; **119:** 2991–3002.
58. Baldridge MT, King KY, Boles NC, *et al*. Quiescent haematopoietic stem cells are activated by IFN-gamma in response to chronic infection. *Nature* 2010; **465:** 793–797.
59. Chiba Y, Mizoguchi I, Hasegawa H, *et al*. Regulation of myelopoiesis by proinflammatory cytokines in infectious diseases. *Cell Mol Life Sci* 2018; **75:** 1363–1376.
60. Kwok AJ, Allcock A, Ferreira RC, *et al*. Neutrophils and emergency granulopoiesis drive immune suppression and an extreme response endotype during sepsis. *Nat Immunol* 2023; **24:** 767–779.
61. Hotchkiss RS, Monneret G, Payen D. Sepsis-induced immunosuppression: from cellular dysfunctions to immunotherapy. *Nat Rev Immunol* 2013; **13:** 862–874.
62. Petty NK, Bulgin R, Crepin VF, *et al*. The Citrobacter rodentium genome sequence reveals convergent evolution with human pathogenic Escherichia coli. *J Bacteriol* 2010; **192:** 525–538.
63. Borenshtein D, Nambiar PR, Groff EB, *et al*. Development of fatal colitis in FVB mice infected with Citrobacter rodentium. *Infect Immun* 2007; **75:** 3271–3281.
64. Brennan PC, Fritz TE, Flynn RJ, *et al*. Citrobacter Freundii associated with diarrhea in a laboratory mice. *Lab Anim Care* 1965; **15:** 266–275.
65. Ediger RD, Kovatch RM, Rabstein MM. Colitis in mice with a high incidence of rectal prolapse. *Lab Anim Sci* 1974; **24:** 488–494.
66. Dieleman LA, Palmen MJ, Akol H, *et al*. Chronic experimental colitis induced by dextran sulphate sodium (DSS) is characterized by Th1 and Th2 cytokines. *Clin Exp Immunol* 1998; **114:** 385–391.
67. Asseman C, Mauze S, Leach MW, *et al*. An essential role for interleukin 10 in the function of regulatory T cells that inhibit intestinal inflammation. *J Exp Med* 1999; **190:** 995–1004.
68. Ostanin DV, Bao J, Koboziev I, *et al*. T cell transfer model of chronic colitis: concepts, considerations, and tricks of the trade. *Am J Physiol Gastrointest Liver Physiol* 2009; **296:** G135–G146.
69. Collins JW, Keeney KM, Crepin VF, *et al*. Citrobacter rodentium: infection, inflammation and the microbiota. *Nat Rev Microbiol* 2014; **12:** 612–623.
70. Chan JM, Bhinder G, Sham HP, *et al*. CD4+ T cells drive goblet cell depletion during Citrobacter rodentium infection. *Infect Immun* 2013; **81:** 4649–4658.
71. Vallejos OP, Bueno SM, Kalergis AM. Probiotics in inflammatory bowel disease: microbial modulation and therapeutic prospects. *Trends Mol Med* 2025; **31:** 731–742.
72. Edrey YH, Hanes M, Pinto M, *et al*. Successful aging and sustained good health in the naked mole rat: a long-lived mammalian model for biogerontology and biomedical research. *ILAR J* 2011; **52:** 41–53.
73. Delaney MA, Imai DM, Buffenstein R. Spontaneous disease and pathology of naked mole-rats. *Adv Exp Med Biol* 2021; **1319:** 353–380.
74. Kamada N, Seo SU, Chen GY, *et al*. Role of the gut microbiota in immunity and inflammatory disease. *Nat Rev Immunol* 2013; **13:** 321–335.
75. Haak BW, Wiersinga WJ. The role of the gut microbiota in sepsis. *Lancet Gastroenterol Hepatol* 2017; **2:** 135–143.
76. Abraham C, Cho JH. Inflammatory bowel disease. *N Engl J Med* 2009; **361:** 2066–2078.
77. Podolsky DK. Inflammatory bowel disease. *N Engl J Med* 2002; **347:** 417–429.
78. Zeng MY, Inohara N, Nunez G. Mechanisms of inflammation-driven bacterial dysbiosis in the gut. *Mucosal Immunol* 2017; **10:** 18–26.
79. Shebzukhov Y, Holtze S, Hirseland H, *et al*. Identification of cross-reactive antibodies for the detection of lymphocytes, myeloid cells and haematopoietic precursors in the naked mole rat. *Eur J Immunol* 2019; **49:** 2103–2110.
80. Kwok I, Becht E, Xia Y, *et al*. Combinatorial single-cell analyses of granulocyte-monocyte progenitor heterogeneity reveals an early Uni-potent neutrophil progenitor. *Immunity* 2020; **53:** 303–318 e305.
81. Hall LJ, Murphy CT, Hurley G, *et al*. Natural killer cells protect against mucosal and systemic infection with the enteric pathogen Citrobacter rodentium. *Infect Immun* 2013; **81:** 460–469.
82. Lin T, Buffenstein R. The unusual immune system of the naked mole-rat. *Adv Exp Med Biol* 2021; **1319:** 315–327.
83. Brenner DJ, Grimont PA, Steigerwalt AG, *et al*. Classification of citrobacteria by DNA hybridization: designation of Citrobacter farmeri sp. nov., Citrobacter youngae sp. nov., Citrobacter braakii sp. nov., Citrobacter werkmanii sp. nov., Citrobacter sedlakii sp. nov., and three unnamed Citrobacter genomospecies. *Int J Syst Bacteriol* 1993; **43:** 645–658.
84. Arens S, Verbist L. Differentiation and susceptibility of Citrobacter isolates from patients in a university hospital. *Clin Microbiol Infect* 1997; **3:** 53–57.
85. Janda JM, Abbott SL, Cheung WK, *et al*. Biochemical identification of citrobacteria in the clinical laboratory. *J Clin Microbiol* 1994; **32:** 1850–1854.
86. Mundy R, MacDonald TT, Dougan G, *et al*. Citrobacter rodentium of mice and man. *Cell Microbiol* 2005; **7:** 1697–1706.
87. Schauer DB, Falkow S. Attaching and effacing locus of a Citrobacter freundii biotype that causes transmissible murine colonic hyperplasia. *Infect Immun* 1993; **61:** 2486–2492.
88. Deng W, Li Y, Vallance BA, *et al*. Locus of enterocyte effacement from Citrobacter rodentium: sequence analysis and evidence for horizontal transfer among attaching and effacing pathogens. *Infect Immun* 2001; **69:** 6323–6335.
89. Lai Y, Rosenshine I, Leong JM, *et al*. Intimate host attachment: enteropathogenic and enterohaemorrhagic Escherichia coli. *Cell Microbiol* 2013; **15:** 1796–1808.
90. Lupp C, Robertson ML, Wickham ME, *et al*. Host-mediated inflammation disrupts the intestinal microbiota and promotes the overgrowth of Enterobacteriaceae. *Cell Host Microbe* 2007; **2:** 204.
91. Barman M, Unold D, Shifley K, *et al*. Enteric salmonellosis disrupts the microbial ecology of the murine gastrointestinal tract. *Infect Immun* 2008; **76:** 907–915.

92. Kamada N, Kim YG, Sham HP, *et al*. Regulated virulence controls the ability of a pathogen to compete with the gut microbiota. *Science* 2012; **336:** 1325–1329.
93. Ritchie ML, Romanuk TN. A meta-analysis of probiotic efficacy for gastrointestinal diseases. *PLoS One* 2012; **7:** e34938.
94. Alfaleh K, Anabrees J, Bassler D, *et al*. Probiotics for prevention of necrotizing enterocolitis in preterm infants. *Cochrane Database Syst Rev* 2011: CD005496.
95. Reid G, Younes JA, Van der Mei HC, *et al*. Microbiota restoration: natural and supplemented recovery of human microbial communities. *Nat Rev Microbiol* 2011; **9:** 27–38.
96. Heuvelin E, Lebreton C, Grangette C, *et al*. Mechanisms involved in alleviation of intestinal inflammation by bifidobacterium breve soluble factors. *PLoS One* 2009; **4:** e5184.
97. Ni Y, Zhang Y, Zheng L, *et al*. Bifidobacterium and lactobacillus improve inflammatory bowel disease in zebrafish of different ages by regulating the intestinal mucosal barrier and microbiota. *Life Sci* 2023; **324:** 121699.
98. Singh S, Bhatia R, Khare P, *et al*. Anti-inflammatory Bifidobacterium strains prevent dextran sodium sulfate induced colitis and associated gut microbial dysbiosis in mice. *Sci Rep* 2020; **10:** 18597.
99. Xu L, Liu B, Huang L, *et al*. Probiotic consortia and their metabolites ameliorate the symptoms of inflammatory bowel diseases in a colitis mouse model. *Microbiol Spectr* 2022; **10:** e0065722.
100. Kumar M, Kissoon-Singh V, Coria AL, *et al*. Probiotic mixture VSL#3 reduces colonic inflammation and improves intestinal barrier function in Muc2 mucin-deficient mice. *Am J Physiol Gastrointest Liver Physiol* 2017; **312:** G34–G45.
101. Tursi A, Brandimarte G, Papa A, *et al*. Treatment of relapsing mild-to-moderate ulcerative colitis with the probiotic VSL#3 as adjunctive to a standard pharmaceutical treatment: a double-blind, randomized, placebo-controlled study. *Am J Gastroenterol* 2010; **105:** 2218–2227.
102. Sood A, Midha V, Makharia GK, *et al*. The probiotic preparation, VSL#3 induces remission in patients with mild-to-moderately active ulcerative colitis. *Clin Gastroenterol Hepatol* 2009; **7:** 1202–1209.
103. Miele E, Pascarella F, Giannetti E, *et al*. Effect of a probiotic preparation (VSL#3) on induction and maintenance of remission in children with ulcerative colitis. *Am J Gastroenterol* 2009; **104:** 437–443.
104. Azer SA, Tuma F. Infectious colitis. In *StatPearls*. Treasure Island (FL), 2025.

SUPPLEMENTARY MATERIAL ONLINE

Figure S1. Schematic representation of sporadic disease outbreak in our NMR colonies that were observed over a period of 72 weeks after a suspected poor biosecurity practice resulted in pathogen transmission and disease onset

Figure S2. Histology of tissues from symptomatic NMRs

Figure S3. Top: phylogenetic relationship of *C. braakii* to various enteric bacteria based on nucleotide sequences of seven housekeeping genes (*adk*, *fumC*, *gyrB*, *icd*, *mdh*, *purA*, and r*ecA*). Bottom: genome sequence homology of *C. braakii* to various enteric bacteria

Figure S4. Representative images of H&E-stained gut rolls

Table S1. List of primary antibodies used